Notes on force of gas on particles in CE simulations

Luke Chamandy

March 26, 2019

1 Calculation of drag force

1.1 Preliminary comments

From Wikipedia: *In fluid dynamics, drag (sometimes called air resistance, a type of friction, or fluid resistance, another type of friction or fluid friction) is a force acting opposite to the relative motion of any object moving with respect to a surrounding fluid.*

So technically, the drag involves the relative velocity between fluid and particle. Thus far, we have not attempted to calculate the relative velocity between particle and gas or its direction. This would involve taking some average over the gas near the particle. But which region should be chosen? Should it be a weighted average? A related issue is that in the Bondi-Hoyle-Lyttleton (BHL) problem, the velocity that goes into the formula for gas dynamical friction is the relative velocity of the particle and the unperturbed ambient medium at infinity. Thus it is non-trivial to calculate or even define, in the simulation, the relative velocity.

To measure from the simulation the component of the gas dynamical friction force along the relative velocity between particle and gas, we do not need the magnitude of the velocity, just the direction.

In any case, we consider two velocities below. Either (i) we measure the component of the force in the direction of the velocity of the particle in the simulation (lab) frame (equal to the relative velocity if the average gas velocity is 0 in the lab frame), or (ii) we measure the component of the force in the direction of the velocity of one particle with respect to the other particle. This would be equal to the relative velocity of particle and gas if the gas was moving along with the other particle. The velocity (ii) is in general greater than (i). In the idealization that the envelope is not rotating and continues to orbit with particle 1 at its center, velocity (ii) would be the relative velocity between particle 2 and gas. The envelope actually would lag the core, so (ii) is probably an overestimate, but on the other hand gas gets accelerated (and slighshotted) as it approaches particle 2. In the early stages, the relative velocity between particle 1 and gas is basically 0, while the velocity between particle 2 and gas is close to velocity (ii) since the envelope is not rotating initially. In the late stages, the relative velocity between each particle and the gas is probably smaller than (i) because of gas round the particle orbiting along with the particle. We can also measure the component of the force tangential to the line joining the particles (the ϕ-component). However, for analytical estimates from BHL theory, we need the magnitude.

To make contact with other approaches for CEE, e.g. MacLeod et al. (2017) to measure the drag force on particle 2, it is reasonable to either use the velocity of particle 2 with respect to particle 1 or the ϕ-component of that velocity. These are the same for circular orbits, and the orbit is approximated to be circular in many studies.

Another possibility is to calculate the orbital velocity of particle 2 with respect to particle 1 at a given separation, assuming that the envelope remains unperturbed, assuming a circular orbit, and taking into account only the envelope mass inside the orbit at a given time and the core mass.

One approach is just to measure the magnitude of the total dynamical friction force from the simulation, which is an upper limit on any individual component of itself.

Then, to take the most favourable value of the relative velocity that would give the smallest value of the drag according to BHL theory. If the BHL force is *still* much larger than the force we measure in the simulation, then we can be sure that simulation and theory do not agree.

1.2 Drag force in simulation (lab) inertial frame

Drag force on particle i:

$$F_{\mathrm{d},i} = \frac{\boldsymbol{f}_i \cdot \boldsymbol{v}_i}{v_i} = \frac{f_{i,x}v_{i,x} + f_{i,y}v_{i,y} + f_{i,z}v_{i,z}}{v_i}, \tag{1}$$

where $\boldsymbol{f}_i$ is the net force exerted on particle i by the gravitational interaction with all gas in the simulation domain,

$$\boldsymbol{f}_i = \mathrm{G}m_i \sum_V \rho(\boldsymbol{s}) \frac{\boldsymbol{s} - \boldsymbol{s}_i}{|\boldsymbol{s} - \boldsymbol{s}_i|^3} d^3 s, \tag{2}$$

where m_i is the mass of particle i, ρ is the gas density, V is the volume of the simulation domain, and $\boldsymbol{s} = x\hat{\boldsymbol{x}} + y\hat{\boldsymbol{y}} + z\hat{\boldsymbol{z}}$ and $\boldsymbol{s}_i = x\hat{\boldsymbol{x}}_i + y\hat{\boldsymbol{y}}_i + z\hat{\boldsymbol{z}}_i$ are the positions of the gas element, and particle, respectively. Also,

$$v_i = |\boldsymbol{v}_i| = (v_{i,x}^2 + v_{i,y}^2 + v_{i,z}^2)^{1/2}. \tag{3}$$

Note that as we have defined it, $F_{\mathrm{d},i} < 0$ means a drag force with magnitude $|F_{\mathrm{d},i}|$, while $F_{\mathrm{d},i} > 0$ means a thrust force.

1.3 Drag force in non-inertial frame of one of the particles

The drag force on particle 2 in the reference frame of particle 1 is given by

$$F_{2,\mathrm{drag},1} = \frac{\boldsymbol{f}_2 \cdot (\boldsymbol{v}_2 - \boldsymbol{v}_1)}{v_{2,1}} = \frac{f_{2,x}(v_{2,x} - v_{1,x}) + f_{2,y}(v_{2,y} - v_{1,y}) + f_{2,z}(v_{2,z} - v_{1,z})}{v_{2,1}}, \tag{4}$$

where

$$v_{2,1} = ((v_{2,x} - v_{1,x})^2 + (v_{2,y} - v_{1,y})^2 + (v_{2,z} - v_{1,z})^2)^{1/2}. \tag{5}$$

The drag force on particle 1 in the reference frame of particle 2 is obtained by interchanging indices 1 and 2.

1.4 ϕ-component of force on particle due to gravitational interaction with gas

For some applications, we would like to calculate the component of the force on particle i due to the gas that is tangential to the line joining the particles and paralle to the orbital plane (which we will assume to be parallel to the $z = 0$ plane–this assumption is normally fine but should be checked for each simulation). Thus, we need to convert from Cartesian (x, y, z) to cylindrical (r, ϕ, z) coordinates and then select the ϕ-component. Define $r = [(x_i - x_j)^2 + (y_i - y_j)^2]^{1/2}$, the unit vector $\hat{\boldsymbol{r}} = [(x_i - x_j)\hat{\boldsymbol{x}} + (y_i - y_j)\hat{\boldsymbol{y}}]/r$ and the projection, in the orbital plane, of the vector from particle j to particle i is $\boldsymbol{r} = r\hat{\boldsymbol{r}}$.

The force in equation (2) can be written as

$$\boldsymbol{f}_i = A\hat{\boldsymbol{r}} + B\hat{\boldsymbol{\phi}} + C\hat{\boldsymbol{z}} \tag{6}$$

We want to know the ϕ-component, that is we want to know the value of B. Then we compute

$$\boldsymbol{r} \times \boldsymbol{f}_i = rB\hat{\boldsymbol{z}} - rC\hat{\boldsymbol{\phi}} \tag{7}$$

and take the z-component. That is,

$$f_{i,\phi} = \frac{\boldsymbol{r} \times \boldsymbol{f}_i}{r} \cdot \hat{\boldsymbol{z}}. \tag{8}$$

Now, since the simulation uses Cartesian coordinates, we want the right side written in Cartesian coordinates. Then

$$f_{i,\phi} = \frac{\boldsymbol{r} \times \boldsymbol{f}_i}{r} \cdot \hat{\boldsymbol{z}} = \frac{r_x f_{i,y} - r_y f_{i,x}}{r} = \frac{r_x f_{i,y} - r_y f_{i,x}}{(r_x^2 + r_y^2)^{1/2}} = \frac{(x_i - x_j)f_{i,y} - (y_i - y_j)f_{i,x}}{[(x_i - x_j)^2 + (y_i - y_j)^2]^{1/2}} \tag{9}$$

Likewise, for the radial component parallel to the xy plane we can write,

$$f_{i,r} = \frac{\boldsymbol{r} \cdot \boldsymbol{f}_i}{r} = \frac{r_x f_{i,x} + r_y f_{i,y}}{r} = \frac{r_x f_{i,x} + r_y f_{i,y}}{(r_x^2 + r_y^2)^{1/2}} = \frac{(x_i - x_j)f_{i,x} + (y_i - y_j)f_{i,y}}{[(x_i - x_j)^2 + (y_i - y_j)^2]^{1/2}}. \tag{10}$$

If we are interested in the force along the axis joining particles 1 and 2 (which need not be in the xy plane in general), this is given by

$$f_{i,R} = \frac{\boldsymbol{r} \cdot \boldsymbol{f}_i}{R} = \frac{(x_i - x_j)f_{i,x} + (y_i - y_j)f_{i,y} + (z_i - z_j)f_{i,z}}{[(x_i - x_j)^2 + (y_i - y_j)^2 + (z_i - z_j)^2]^{1/2}}. \tag{11}$$

The ϕ-, r- and R-components of the velocity can be calculated in precisely the same way as the forces.

2 Results

2.1 Comparison of forces obtained using different simulation analysis tools

Table 1: Comparison between values of force components for frame 173 (last frame of simulation, at $t = 40\,\mathrm{d}$), for three different analysis methods: Post-processing using AstroBear (Astrobear PP), VisIt analysis on full simulation data (VisIt full), and the same VisIt analysis on deresolved simulation data (VisIt deresolved).

Component	AstroBear PP	VisIt full	VisIt deresolved
$f_{1,x}$	1.3207×10^{34}	1.3209×10^{34}	1.316×10^{34}
$f_{1,y}$	-8.5798×10^{33}	-8.5806×10^{34}	-8.652×10^{34}
$f_{1,z}$	-3.4892×10^{32}	-3.4959×10^{32}	-3.214×10^{32}
$f_{2,x}$	-1.2274×10^{34}	-1.2274×10^{34}	-1.251×10^{34}
$f_{2,y}$	4.5818×10^{33}	4.5834×10^{33}	4.576×10^{33}
$f_{2,z}$	2.1299×10^{32}	2.1019×10^{32}	-2.918×10^{31}

See Tab. 2.1. The values of the force components for frame 173 (last frame of simulation at $t = 40\,\mathrm{d}$) agree very well between post-processing and VisIt tools for the full resolution data ($< 0.04\%$ difference for x- and y-components). It was

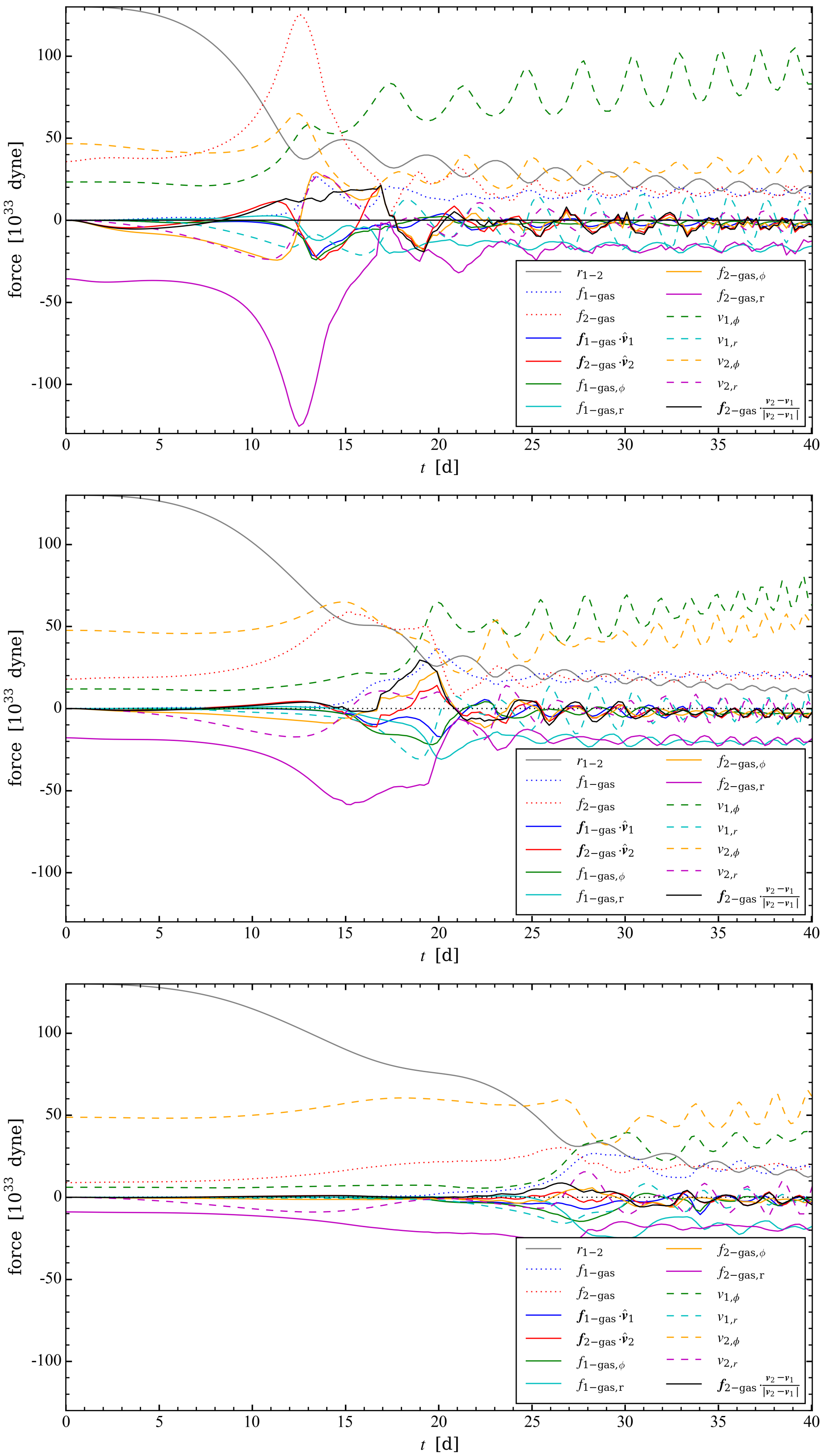

Figure 1: Force $\boldsymbol{f}_i \cdot \boldsymbol{v}/v$ and components of $\boldsymbol{f}_i$ for both particles, with inter-particle separation curve plotted in grey for reference. Velocity components for each particle are also plotted for reference (with an arbitrary linear scale). Note that positive r-component means away from the other particle, while positive ϕ-component means in the sense of the orbit. **Top:** Run 143, Fiducial run (Model A of Papers I and II). **Middle:** Run 149 with secondary mass half that of fiducial run. **Bottom:** Run 151 with secondary mass one fourth that of fiducial run.

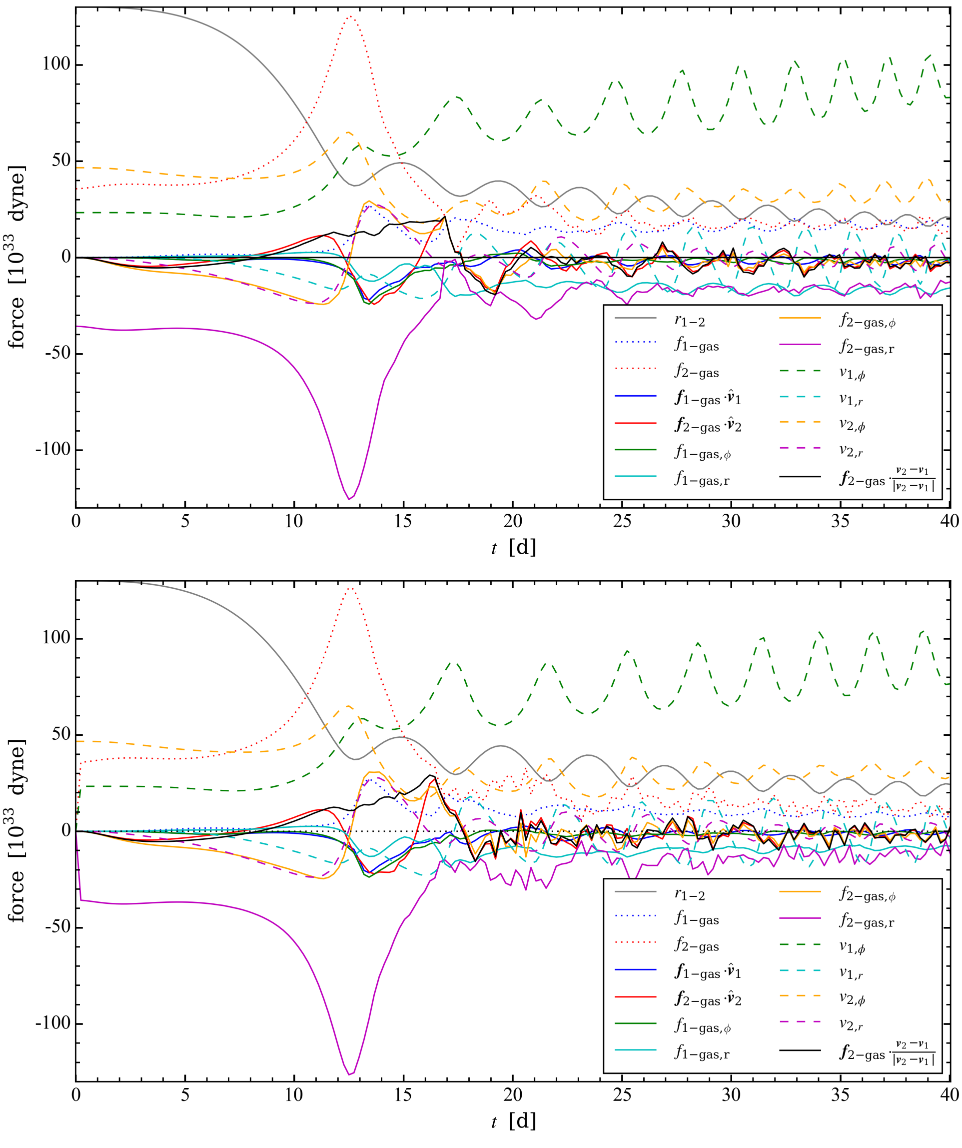

Figure 2: **Top:** Run 143, Fiducial run (Model A of Papers I and II). **Bottom:** Run 132, same as fiducial run except with subgrid accretion model activated (Model B of Paper I).

not possible (due to memory limitations on both Bluehive and Stampede 2) to complete the VisIt analysis using the full data set, but we could do it by first de-resolving the dataset (including only up to maxlevel=3 instead of maxlevel=4 or 5). The agreement for frame 173 is also reasonble between post-processing and VisIt using deresolved data (at the level of 1-2% difference). The figures on the blog post of January 29, 2019 were done using the de-resolved data, analyzed using VisIt. I've redone those figures using postprocessed data and compared the two sets of figures by eye (AstroBear post-processing and VisIt de-resolved) and differences are fairly negligible.

2.2 Force as a function of time

Fig. 1: Force on secondary in frame of primary $\boldsymbol{f}_2 \cdot \boldsymbol{v}/v$ is shown by black line. Phi-component $f_{2,\phi}$ is shown by orange line. Note that at early times, $\boldsymbol{f}_2 \cdot \boldsymbol{v}$ is dominated by $f_{2,r}v_r$ since $f_{2,r}$ is so large. At later times the orange and black lines coincide, so $\boldsymbol{f}_2 \cdot \boldsymbol{v}$ is dominated by $f_{2,\phi}v_\phi$. We see that the ϕ-component of the force (orange) is positive during plunge-in (so of opposite sign to the predicted drag force). The secondary is being accelerated around in its orbit by the posterior side of the envelope, which lags the primary particle in its orbit (paper 2). Subsequently, the force is mostly a drag force (-ve ϕ component) but the ϕ component actually oscillates from positive to negative .

2.3 Importance of z-components

Fig. 3: We compare the vertical components of the gas gravitational force on each particle and velocity of each particle with the component parallel to the orbital plane. We also compare the difference in vertical positions of the particles with the magnitude of their projected separation in the orbital plane. Finally we compare the components of the gravitational force of gas on each particle and particle velocity along the line separating the particles (subscript R) with its projection on the orbital plane (subscript r). Since these latter quantities turn out to be very small we multiply by 10 in the plot. We see that the vertical components are small, except, at times, the vertical gas force on particle 2, which has a maximum value of 19% of the component parallel to the orbital plane (light blue).

2.4 Velocities

Fig. 5: Velocities of the particles are calculated in two different ways. Either they are computed directly from the simulation data or they are calculated assuming a circular two-body orbit between the secondary and the mass of the primary that would be inside the actual orbit at time t had the envelope retained its original profile (velocities denoted by subscript '0').

$$v_{1,0} = \sqrt{\frac{Gm_2}{a}}\sqrt{\frac{m_2}{m_1+m_2}} = \sqrt{\frac{G\mu}{a}}\sqrt{\frac{m_2}{m_1}}, \tag{12}$$

where

$$\mu \equiv \frac{m_1 m_2}{m_1+m_2} \tag{13}$$

is the reduced mass. By symmetry,

$$v_{2,0} = \sqrt{\frac{Gm_1}{a}}\sqrt{\frac{m_1}{m_1+m_2}} = \sqrt{\frac{G\mu}{a}}\sqrt{\frac{m_1}{m_2}}, \tag{14}$$

and the velocites are in opposite directions. Note that here m_1 is the value of the interior envelope mass + core.

We see that the two different ways of calculating the velocities yield results that are in reasonable agreement.

2.5 Analytical expression for drag force

To obtain an analytical expression for the drag force on particle 2, we made use of the Bondi-Hoyle-Lyttleton formalism, and we considered different variations on that formalism (Edgar, 2004). Three quantities are needed for this: the particle velocity with respect to the ambient velocity of gas (formally the relative particle-gas velocity at infinity), the ambient gas density (formally the gas density at infinity), and the ambient sound speed (formally the gas sound speed at infinity).

To estimate the particle-gas velocity for gas at infinity, we have used the actual velocity of the particle either in the simulation (lab) frame or in the frame of the other particle (see Sec. 1) or we have used the velocity for a circular orbit at the actual separation assuming that the envelope still retained its initial profile.

To estimate the gas density at infinity, we have used the density at the actual separation in the initial envelope profile $\rho_0[a(t)]$.

To estimate the sound speed at infinity, we have used the sound speed at the actual separation in the initial envelope profile $c_0[a(t)]$, that is

$$c_0 = \left(\gamma\frac{P_0}{\rho_0}\right)^{1/2}, \tag{15}$$

where $\gamma = 5/3$ in our simulation, and P_0 and ρ_0 are taken from the original 1D MESA profile.

Analytical and semi-analytical expresions of the force are plotted against time in **Fig. 7**. The low density is predicted to cause the drag force to be negligible at early times.

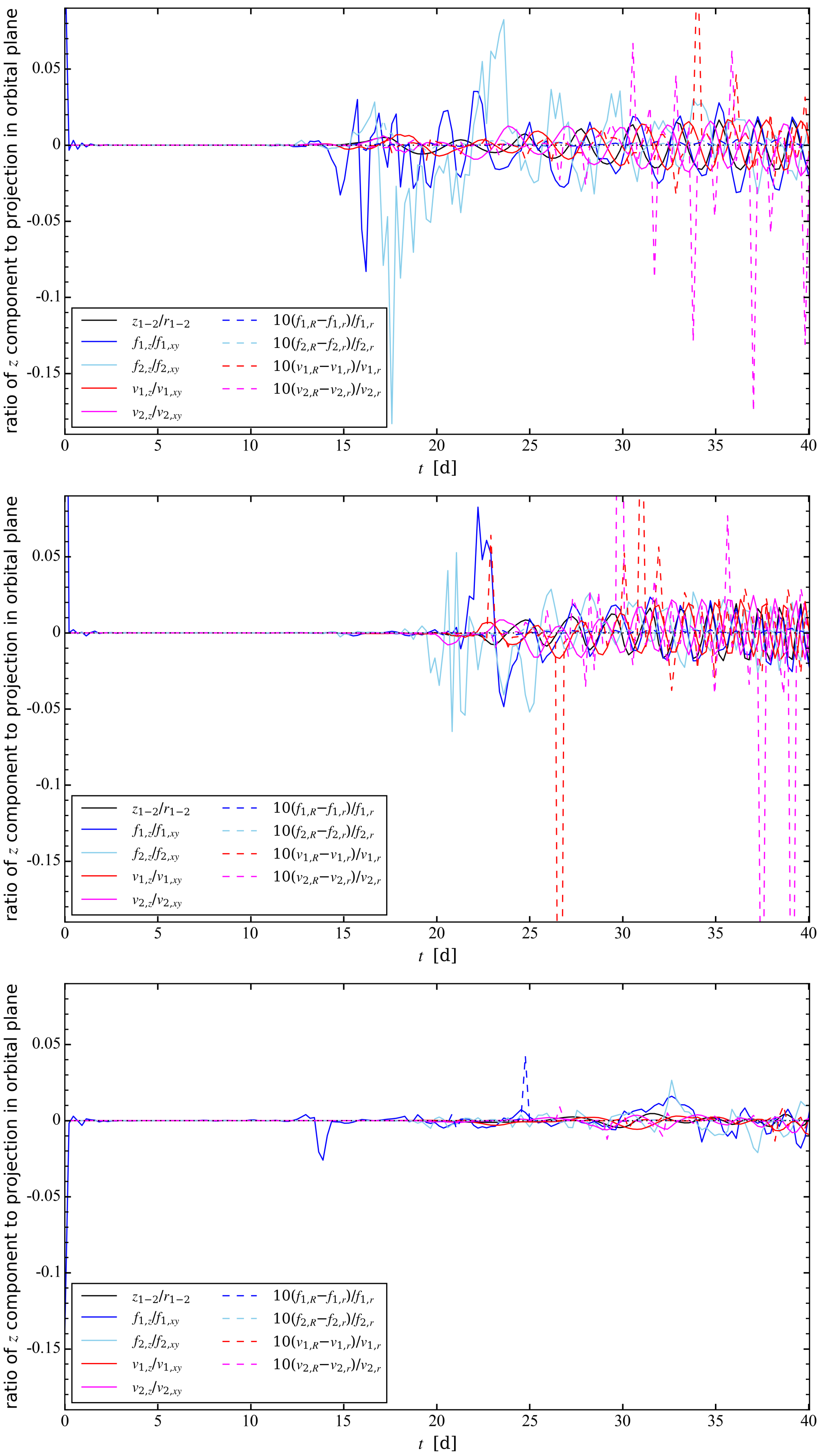

Figure 3: Ratios of various quantities plotted to gauge importance of vertical (z) component as compared to component in orbital (xy) plane. **Top:** Run 143, Fiducial run (Model A of Papers I and II). **Middle:** Run 149 with secondary mass half that of fiducial run. **Bottom:** Run 151 with secondary mass one fourth that of fiducial run.

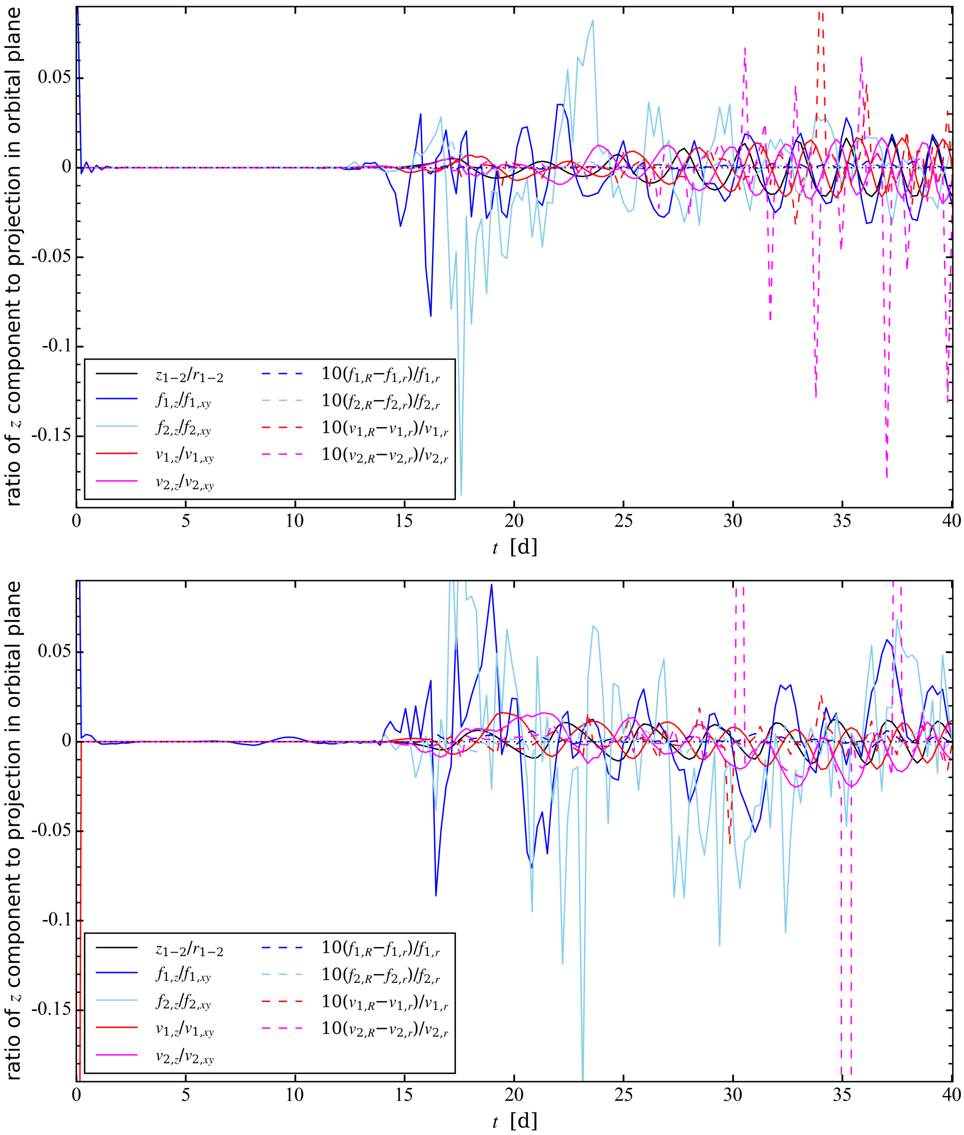

Figure 4: **Top:** Run 143, Fiducial run (Model A of Papers I and II). **Bottom:** Run 132, same as fiducial run except with subgrid accretion model activated (Model B of Paper I).

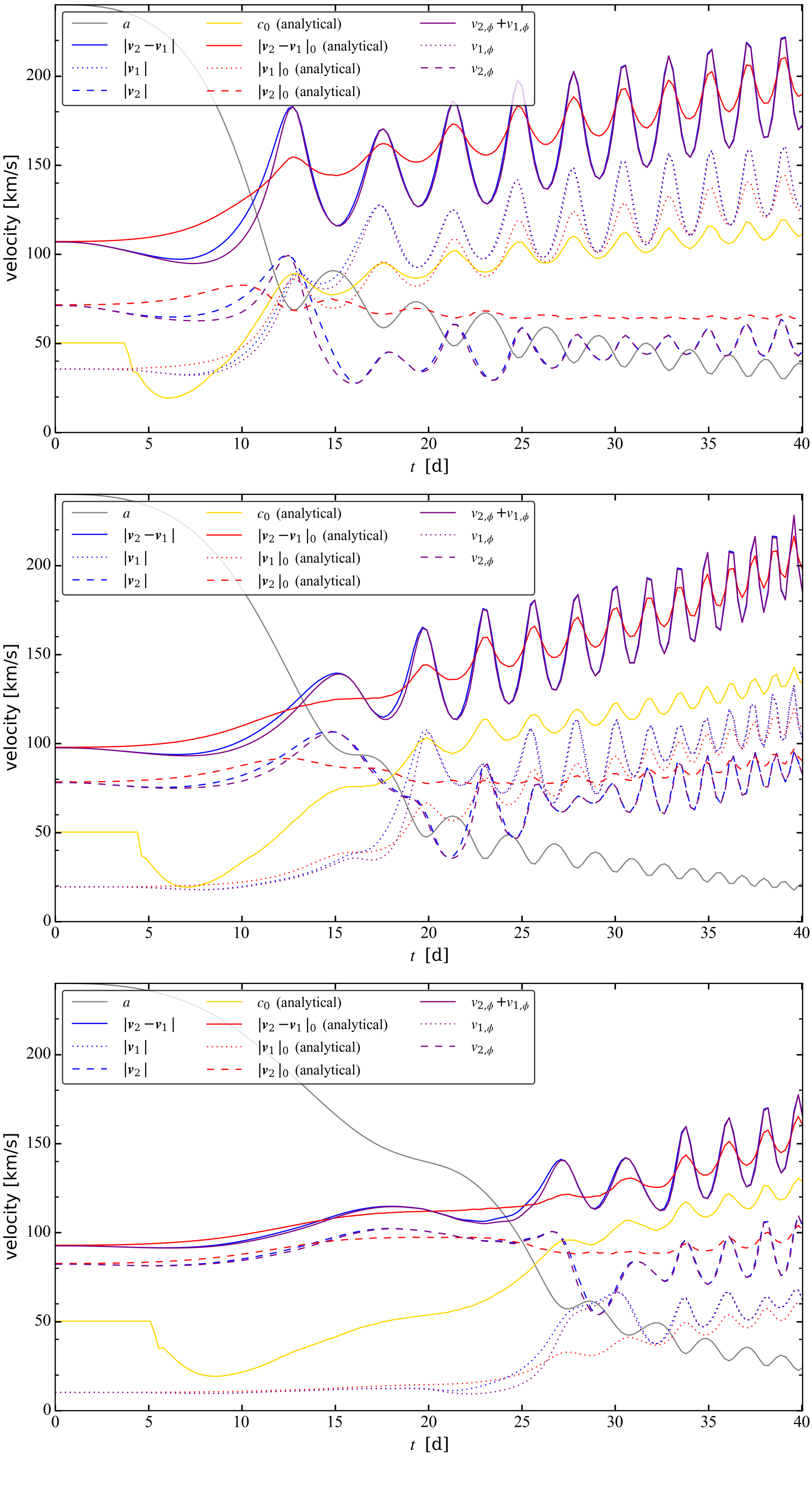

Figure 5: Particle velocities calculated from the simulation or estimated using initial profile. Those quantities estimated from the initial stellar profile are labeled with a '0' subscript. **Top:** Run 143, Fiducial run (Model A of Papers I and II). **Middle:** Run 149 with secondary mass half that of fiducial run. **Bottom:** Run 151 with secondary mass one fourth that of fiducial run.

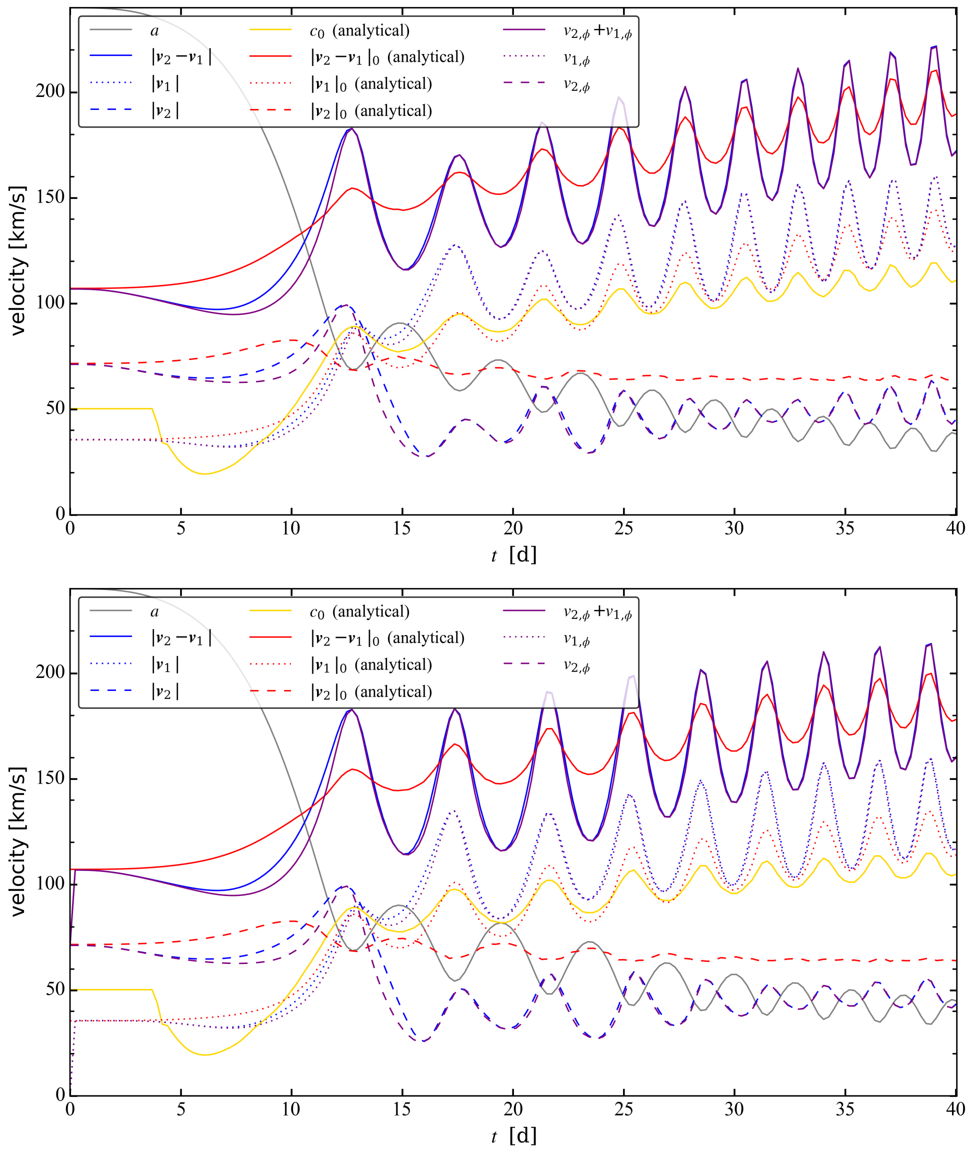

Figure 6: **Top:** Run 143, Fiducial run (Model A of Papers I and II). **Bottom:** Run 132, same as fiducial run except with subgrid accretion model activated (Model B of Paper I).

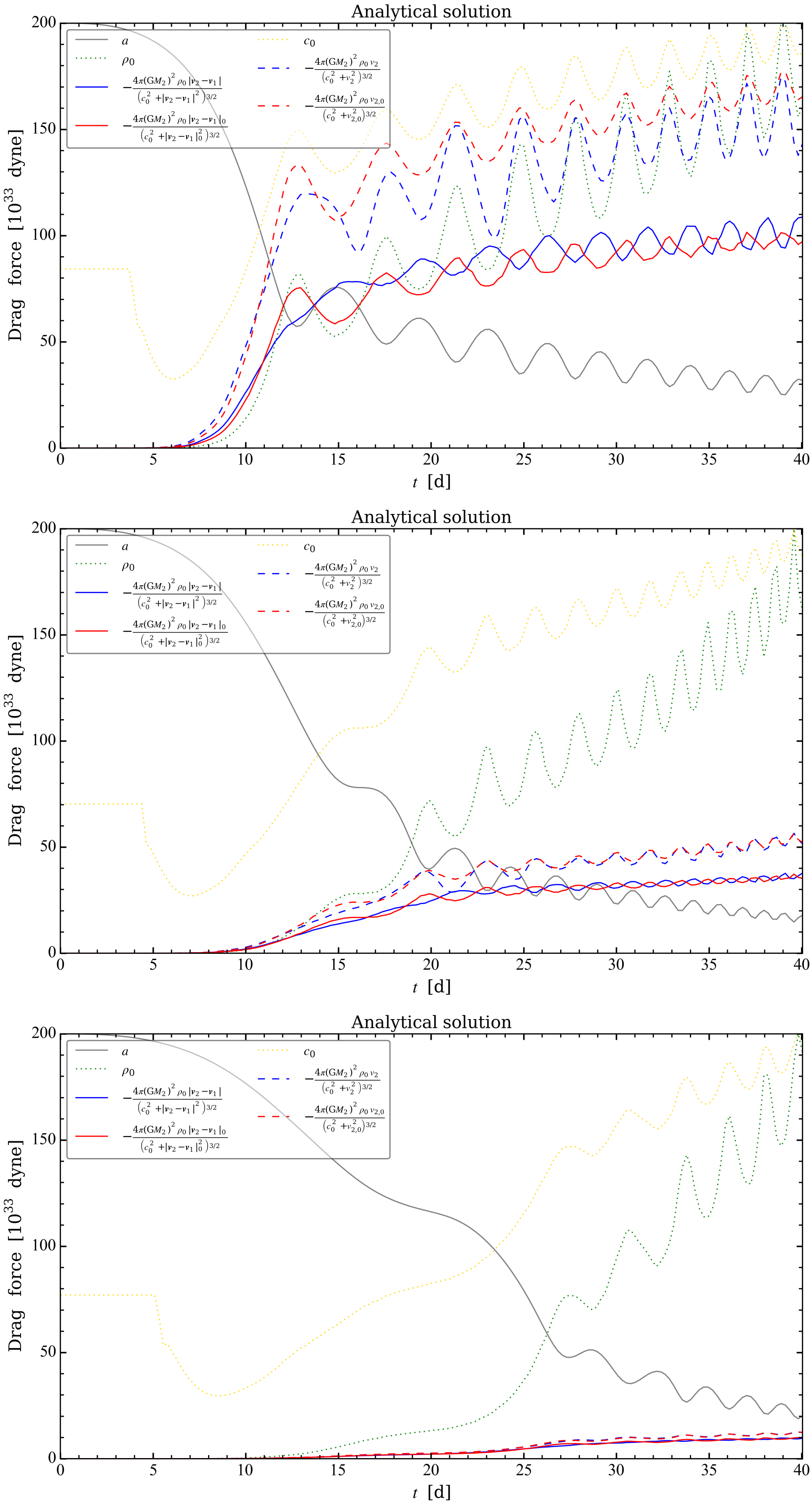

Figure 7: Drag force is now calculated using analytic formula, either with velocity inputted from simulation or else calculated assuming a circular obit between the secondary and the primary mass that would have been interior to $a(t)$ had the envelope remained unperturbed. Density and sound speed are equal to the values in the initial RGB profile, at radius equal to the current inter-particle separation $a(t)$. Density, relative speed and inter-particle separation are plotted for reference (with arbitrary linear scales; density and speed increase with time while separation decreases). **Top:** Run 143, Fiducial run (Model A of Papers I and II). **Middle:** Run 149 with secondary mass half that of fiducial run. **Bottom:** Run 151 with secondary mass one fourth that of fiducial run.

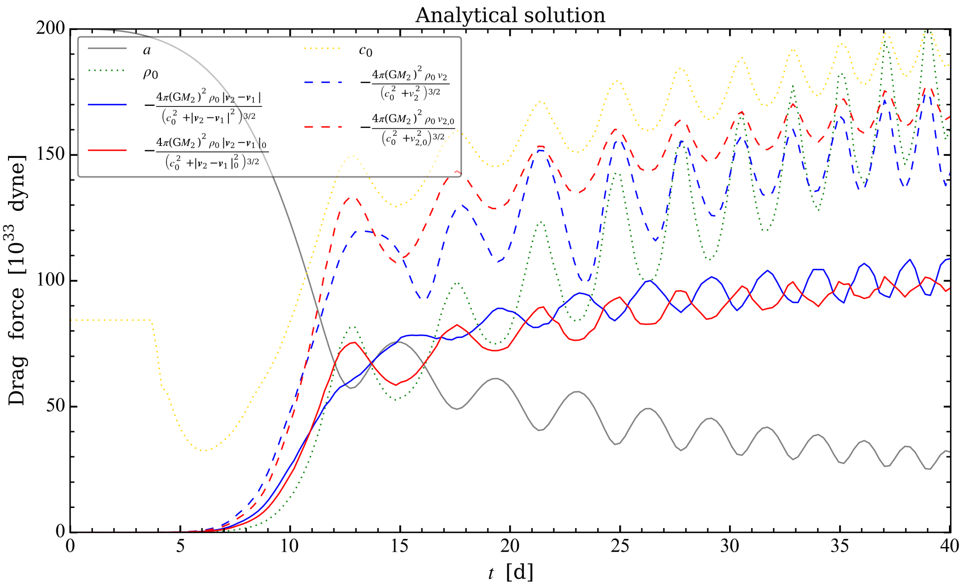

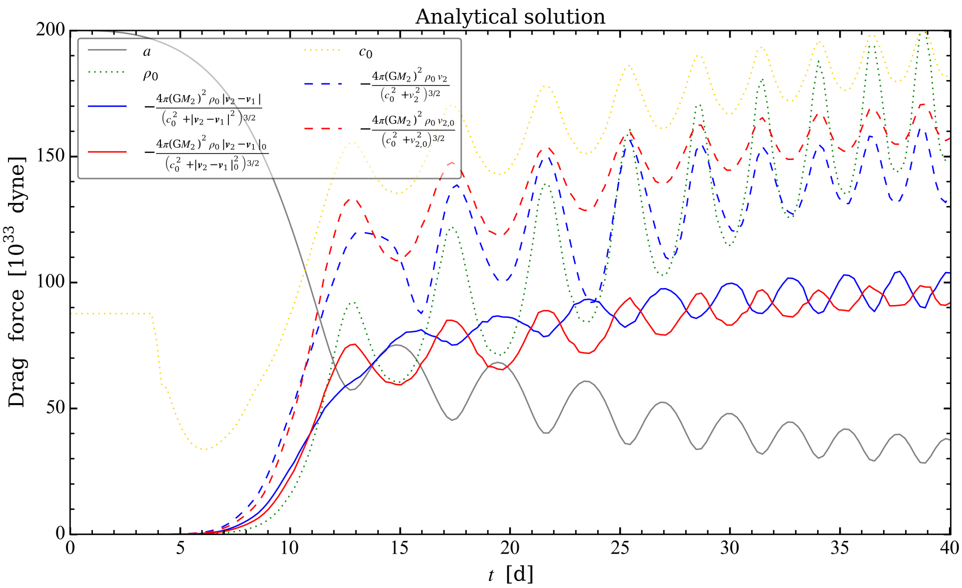

Figure 8: **Top:** Run 143, Fiducial run (Model A of Papers I and II). **Bottom:** Run 132, same as fiducial run except with subgrid accretion model activated (Model B of Paper I).

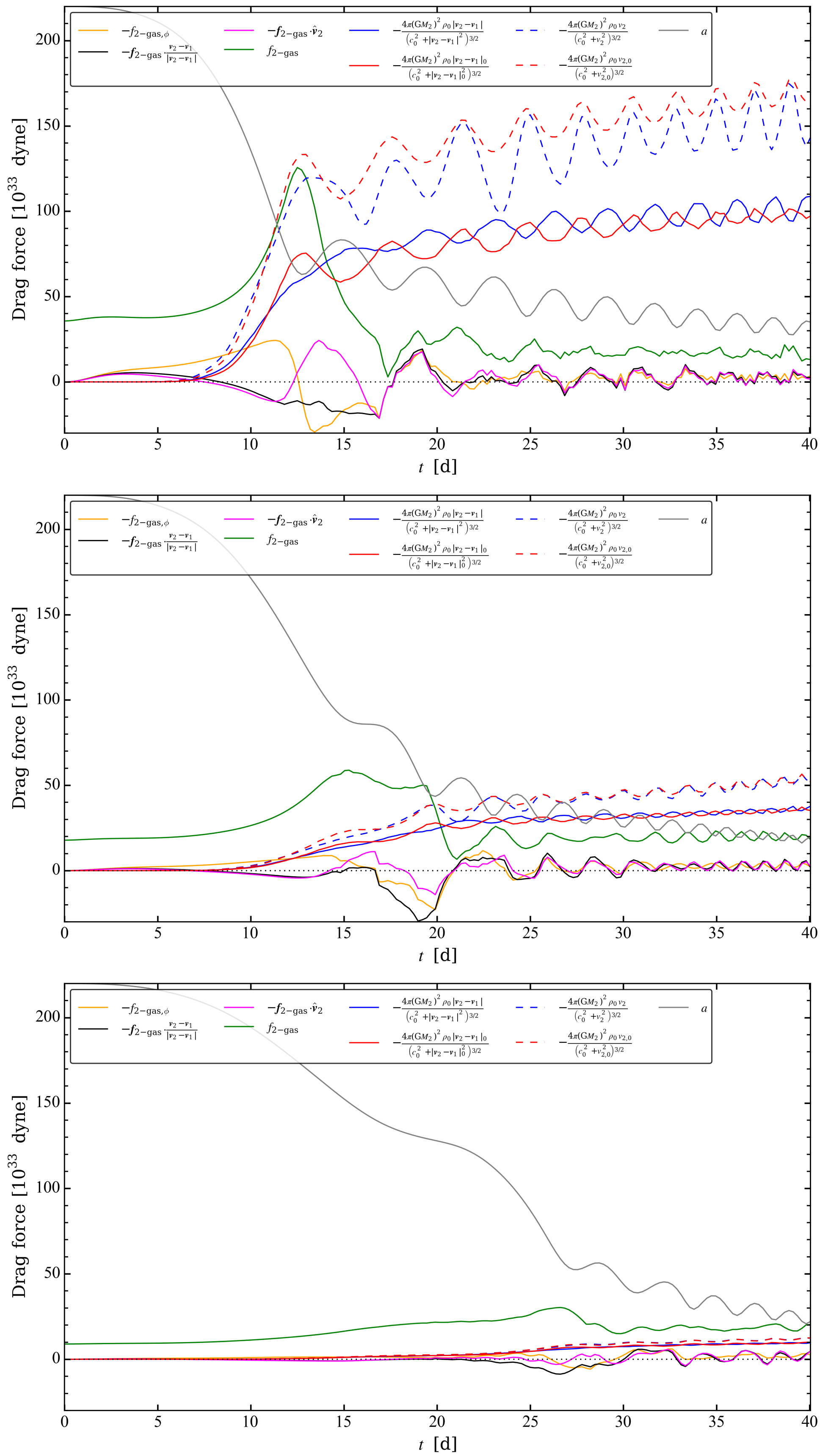

Figure 9: Combination of curvers from Figs. 1 and 7, showing a comparison between the numerical measurements of the 'drag' force (orange, black or magenta) and the analytic (red) or semi-analytic (blue) estimates. The drag force computed from the simulation is much smaller in magnitude, and is sometimes a thrust rather than a drag (negative values on plot). **Top:** Run 143, Fiducial run (Model A of Papers I and II). **Middle:** Run 149 with secondary mass half that of fiducial run. **Bottom:** Run 151 with secondary mass one fourth that of fiducial run.

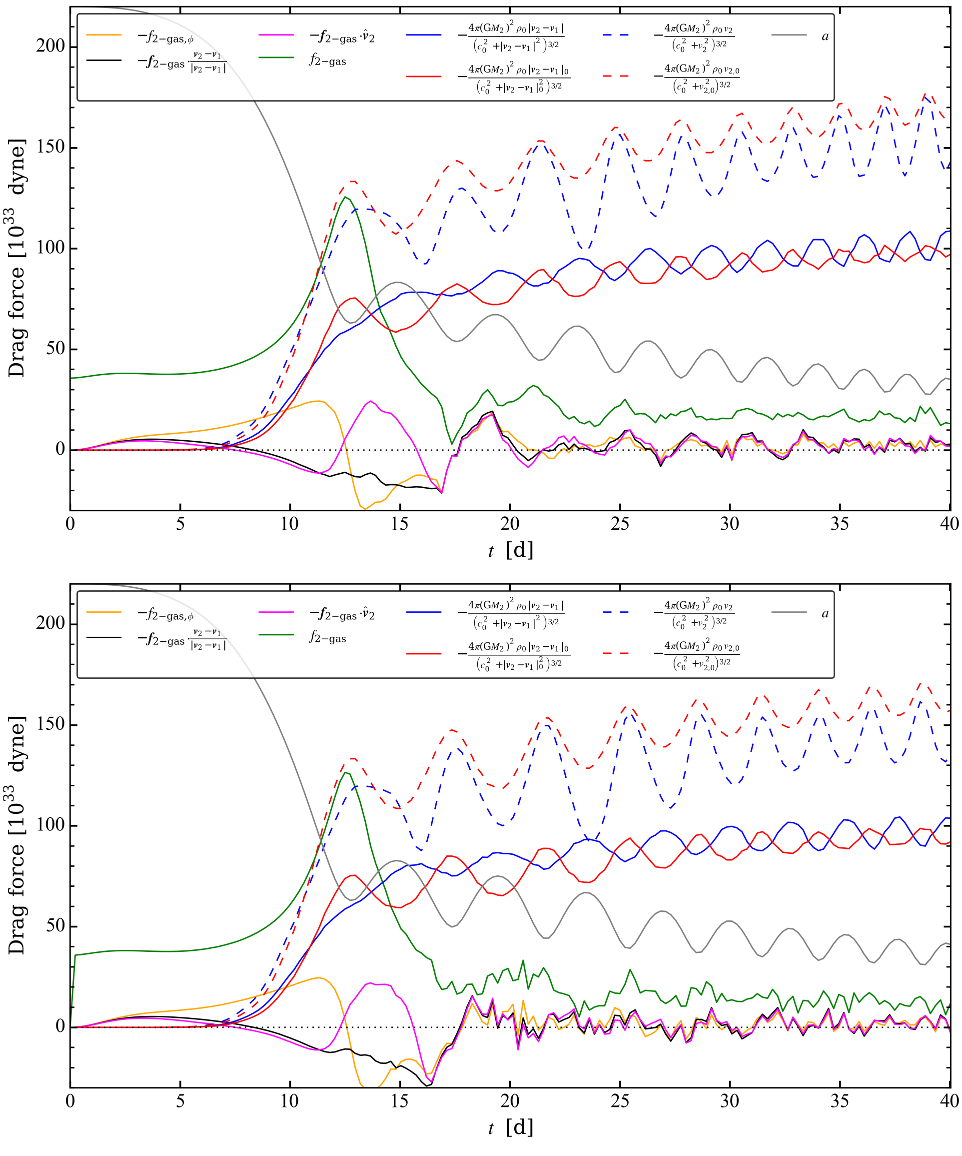

Figure 10: **Top:** Run 143, Fiducial run (Model A of Papers I and II). **Bottom:** Run 132, same as fiducial run except with subgrid accretion model activated (Model B of Paper I).

In **Fig. 9** we plot numerical, analytical and semi-analytical drag force on the same plot. Note that negative values on the graph correspond to thrusts.

The forces from Fig. 1 are normalized to the semi-analytical expressions of Fig. 7 in **Fig. 11**. During the slow spiral-in phase, the magnitude of the drag force is of order $\sim 5\%$ of the predicted value from BHL theory. Note that negative values on the graph correspond to thrusts.

2.6 Bondi-Hoyle radius

Various alternate expressions for the Bondi radius for particles 1 and 2 is plotted in **Fig. 13**. For all definitions, a uniform medium is assumed. That is, the density and pressure gradients are neglected. Also, the initial sound speed of the original profile is assumed. Even more problematic, the envelope is assumed to be stationary in the frame in which the Bondi radius is computed (lab frame or frame of primary point particle). The most relevant Bondi radius curve is probably the one represented by the thick solid red curve, corresponding to the Bondi radius around the secondary in the frame of the primary, including the sound speed in the denominator.

We plot a smaller number of curves in **Fig. 15**, showing the Bondi radius for particle 2 only, with thick lines using the velocity of particle 2 with respect to particle 1 and thin lines using the velocity of particle 1 in the lab frame. Blue means the velocity is computed directly from the simulation, while red means that the velocity is estimated using the initial stellar profile. Focusing on the thick lines, we see that $R_{2,\mathrm{BH}}(t)$ is comparable to $a(t)$ (grey) and comparable to the pressure scale height of the initial profile $H_0[a(t)]$ (green), given by

$$H_0 = -P_0/(dP_0/dr)_0. \tag{16}$$

The density scale height $H_{\rho,0} = -\rho_0/(d\rho_0/dr)_0$ is comparable to H_0, but slightly larger.

Thus, applying the Bondi-Hoyle-Lyttleton formalism to this case is rather questionable. However, it remains to be seen whether applying this formalism would be more justified as M_2 is reduced (in the limit $M_2 \to 0$, $R_{\mathrm{BH}} \to 0$ since $v \sim (\mathrm{G}M_1/a)^{1/2}$, is independent of M_2 in that limit). This can be tested with Runs 149 and 151 which have M_2 equal to 1/2 and 1/4 of the value in the fiducial run (Run 143) plotted here.

References

Edgar R., 2004, New Astron. Rev., 48, 843

MacLeod M., Antoni A., Murguia-Berthier A., Macias P., Ramirez-Ruiz E., 2017, ApJ, 838, 56

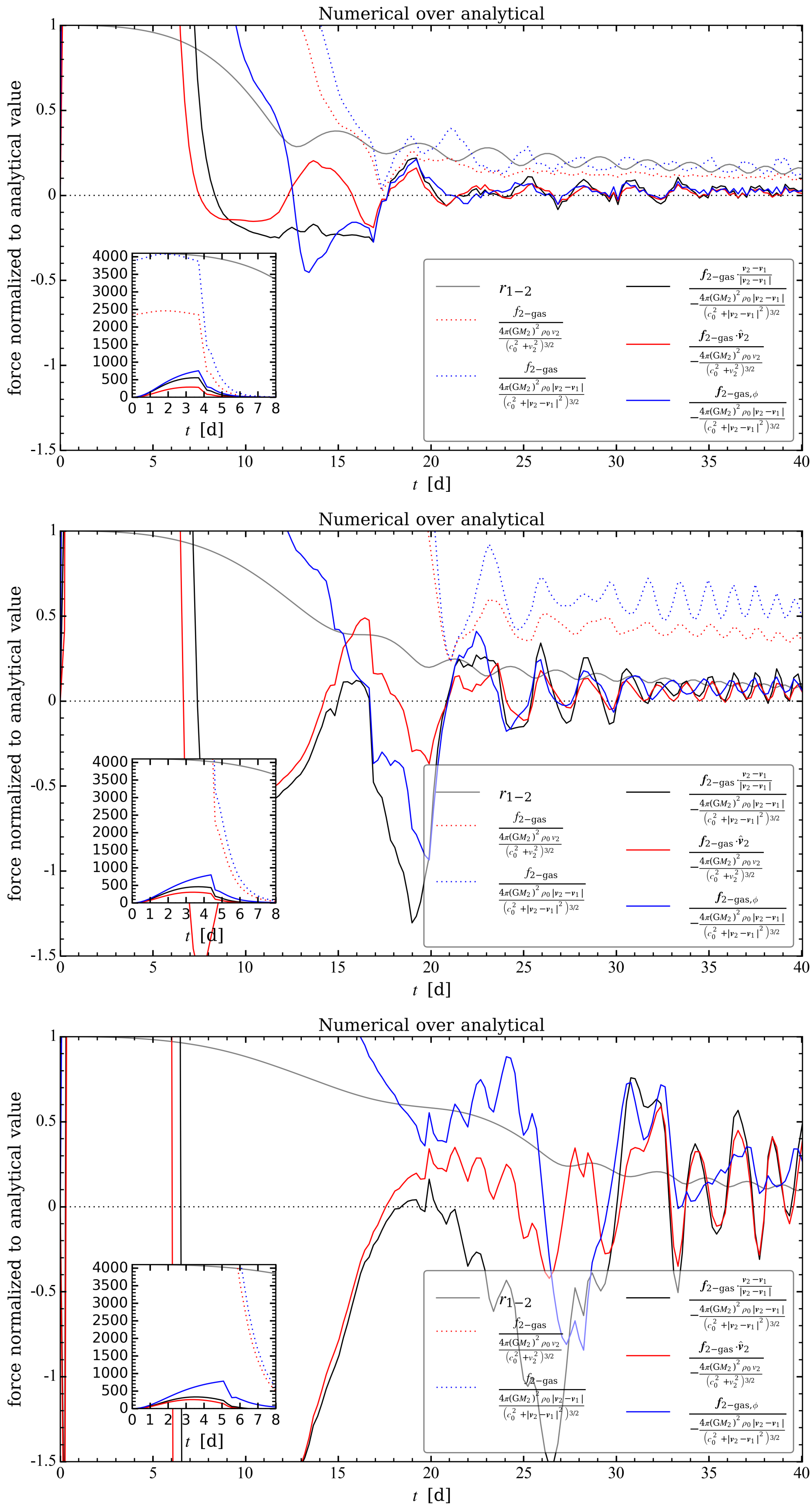

Figure 11: Numerical solution for force component along velocity normalized by semi-analytical drag force solution for a few choices of formulae. Negative values on plot imply a thrust rather than a drag. **Top:** Run 143, Fiducial run (Model A of Papers I and II). **Middle:** Run 149 with secondary mass half that of fiducial run. **Bottom:** Run 151 with secondary mass one fourth that of fiducial run.

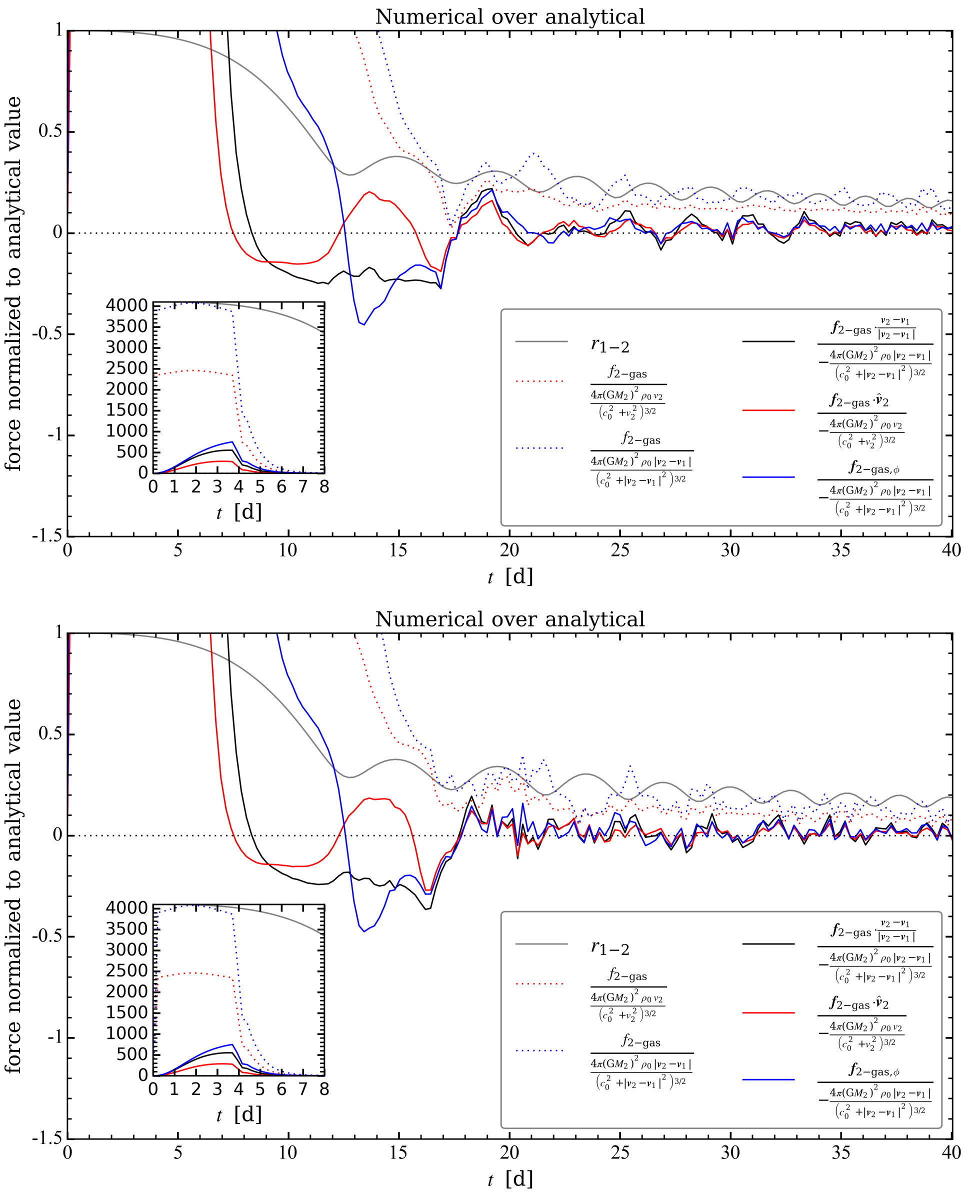

Figure 12: **Top:** Run 143, Fiducial run (Model A of Papers I and II). **Bottom:** Run 132, same as fiducial run except with subgrid accretion model activated (Model B of Paper I).

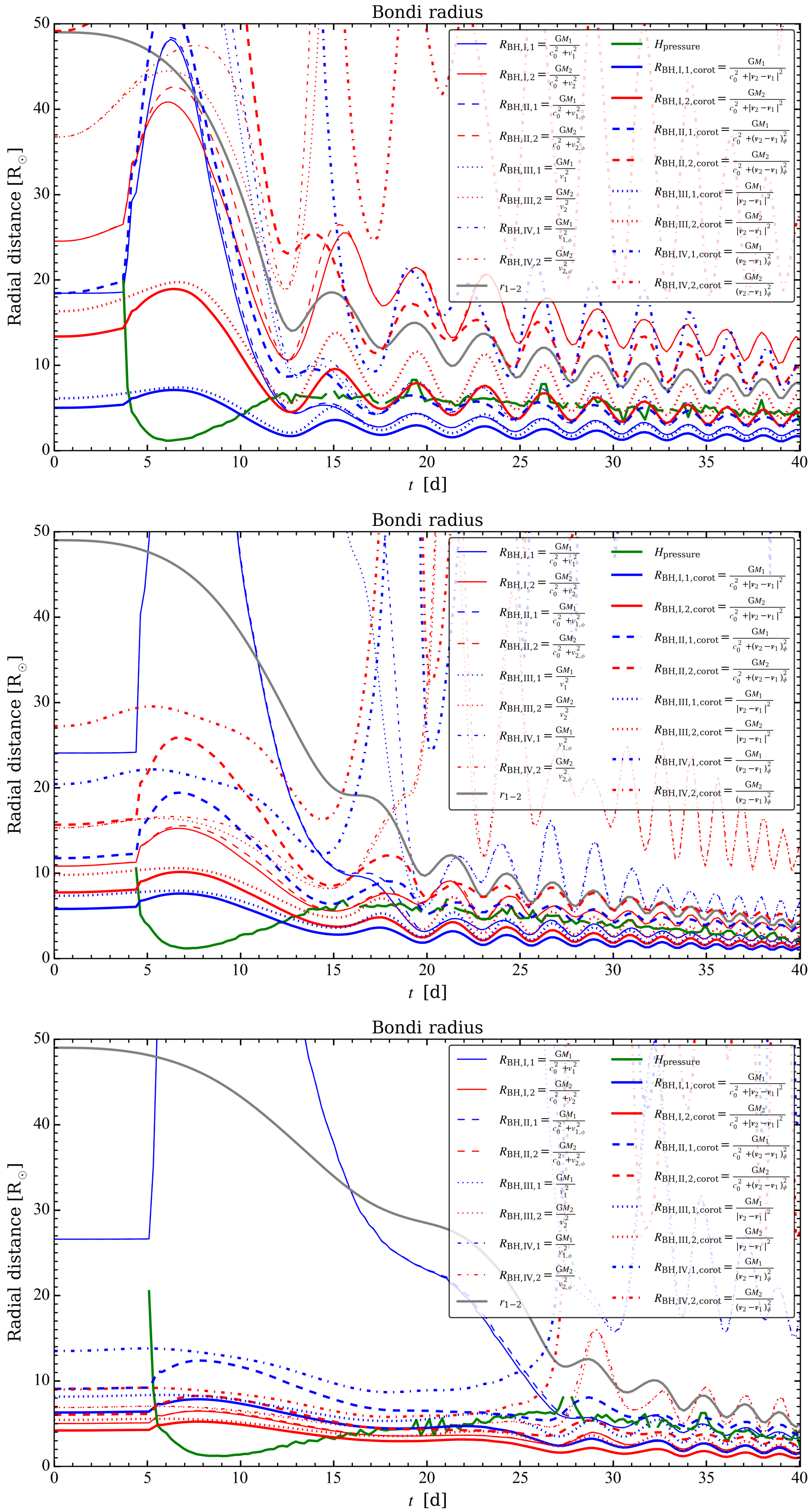

Figure 13: Various definitions of Bondi radius plotted for both particles. Also plotted for reference are the inter-particle separation (grey) and pressure scale height of the original RGB profile at $r = a(t)$. **Top:** Run 143, Fiducial run (Model A of Papers I and II). **Middle:** Run 149 with secondary mass half that of fiducial run. **Bottom:** Run 151 with secondary mass one fourth that of fiducial run.

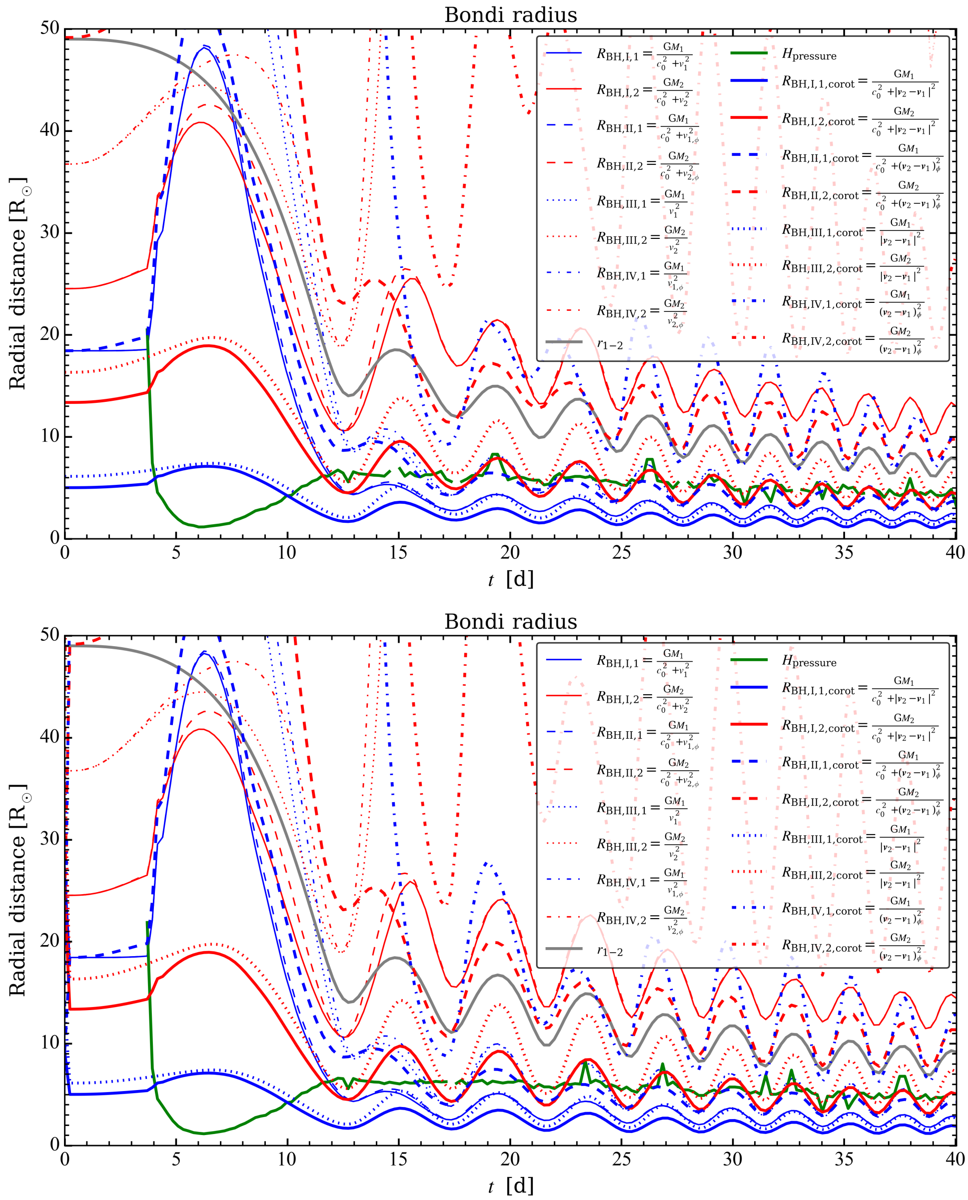

Figure 14: **Top:** Run 143, Fiducial run (Model A of Papers I and II). **Bottom:** Run 132, same as fiducial run except with subgrid accretion model activated (Model B of Paper I).

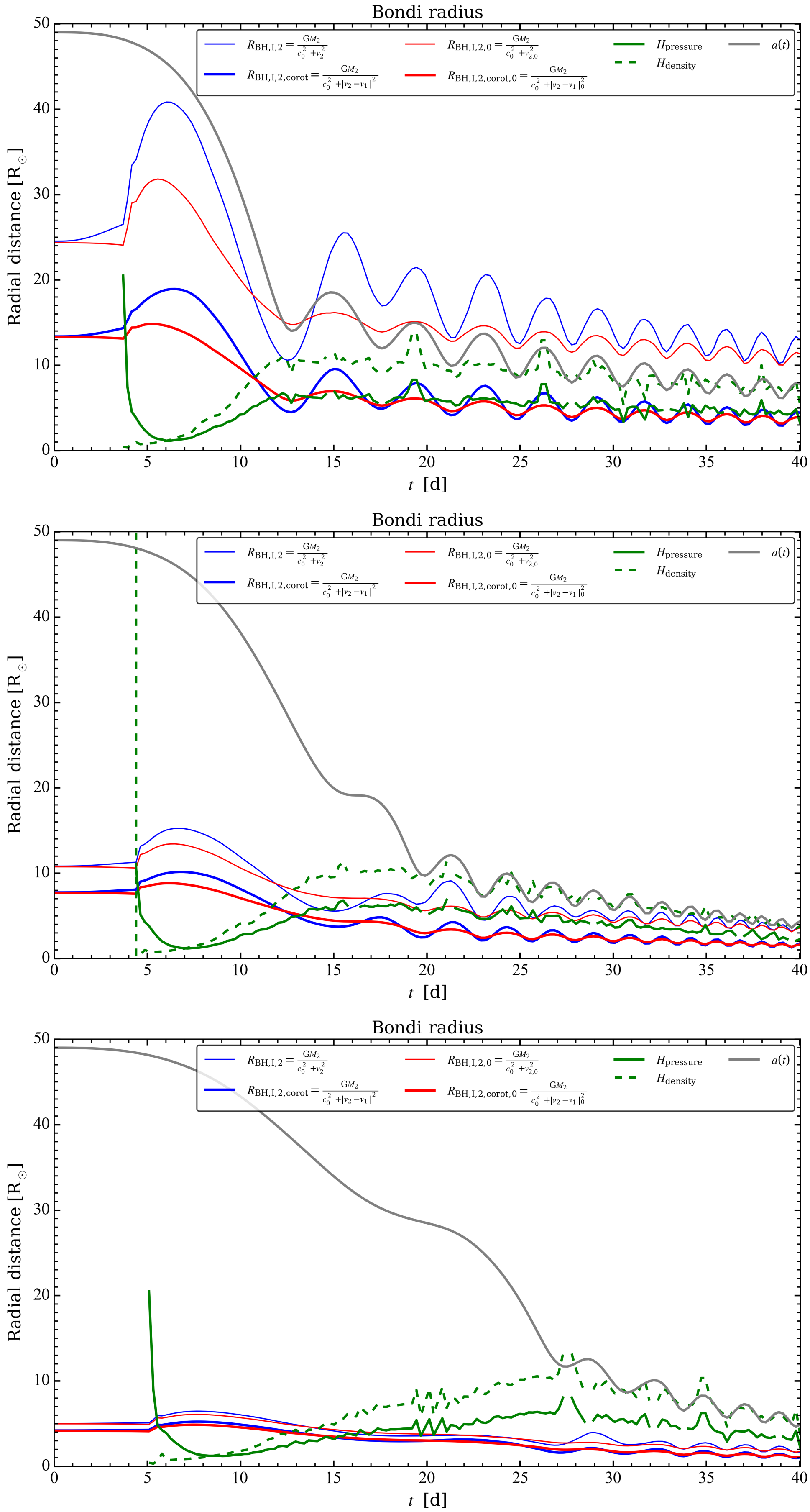

Figure 15: Focusing on two of the definitions for particle 2 from Fig. 13 (blue), but now also showing the same quantities calculated using the analytically calculated velocities (red). **Top:** Run 143, Fiducial run (Model A of Papers I and II). **Middle:** Run 149 with secondary mass half that of fiducial run. **Bottom:** Run 151 with secondary mass one fourth that of fiducial run.

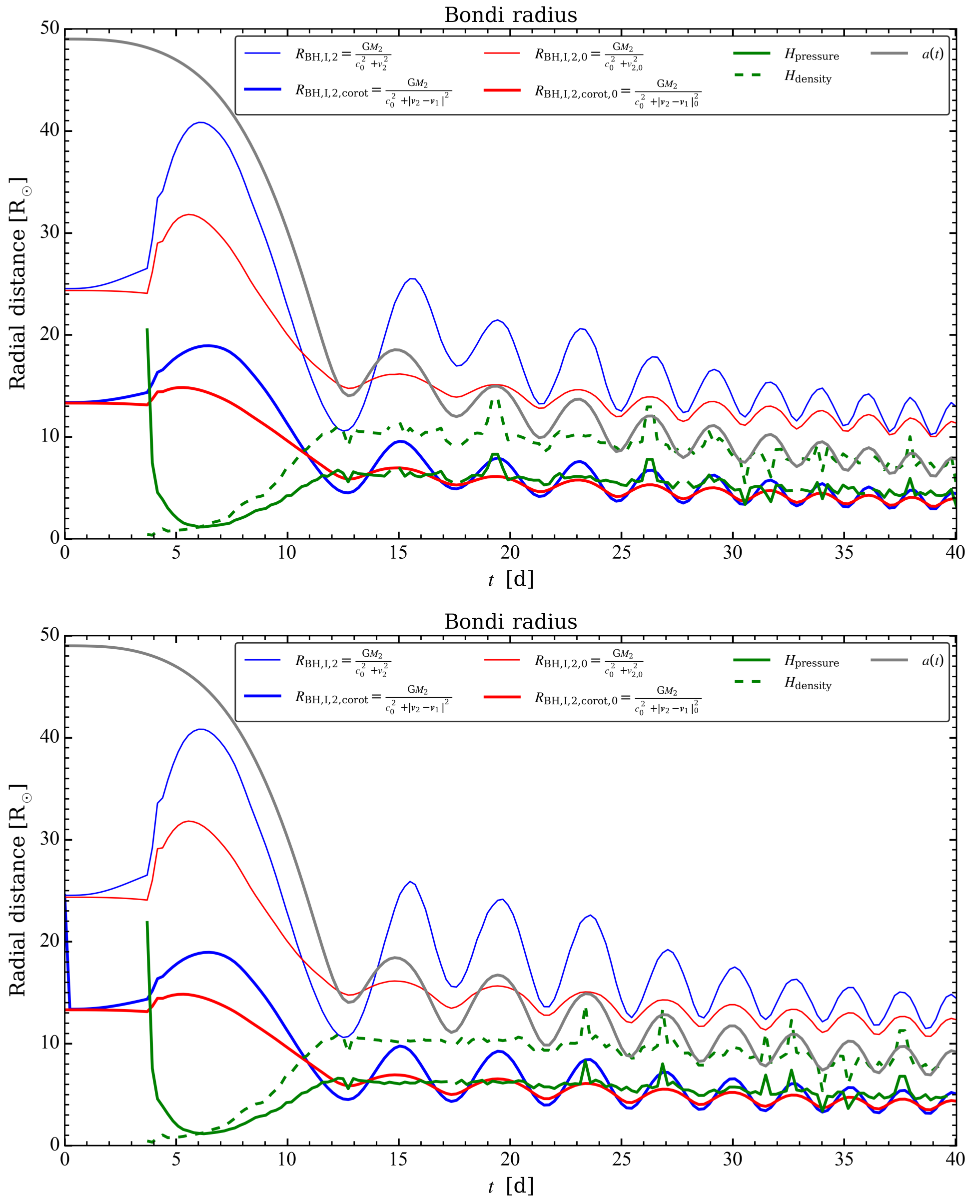

Figure 16: **Top:** Run 143, Fiducial run (Model A of Papers I and II). **Bottom:** Run 132, same as fiducial run except with subgrid accretion model activated (Model B of Paper I).

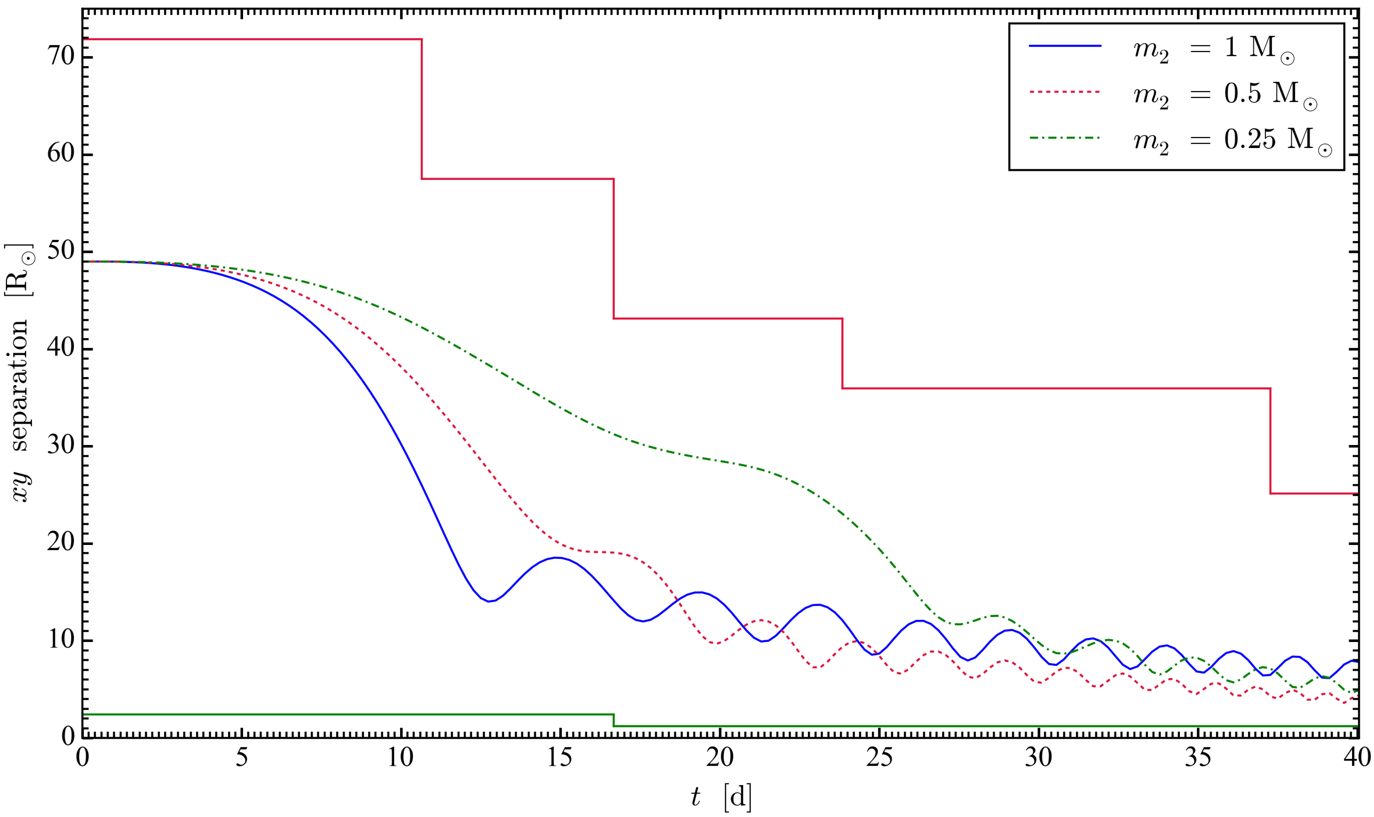

Figure 17: $a(t)$ for Runs 143, 149 and 151.

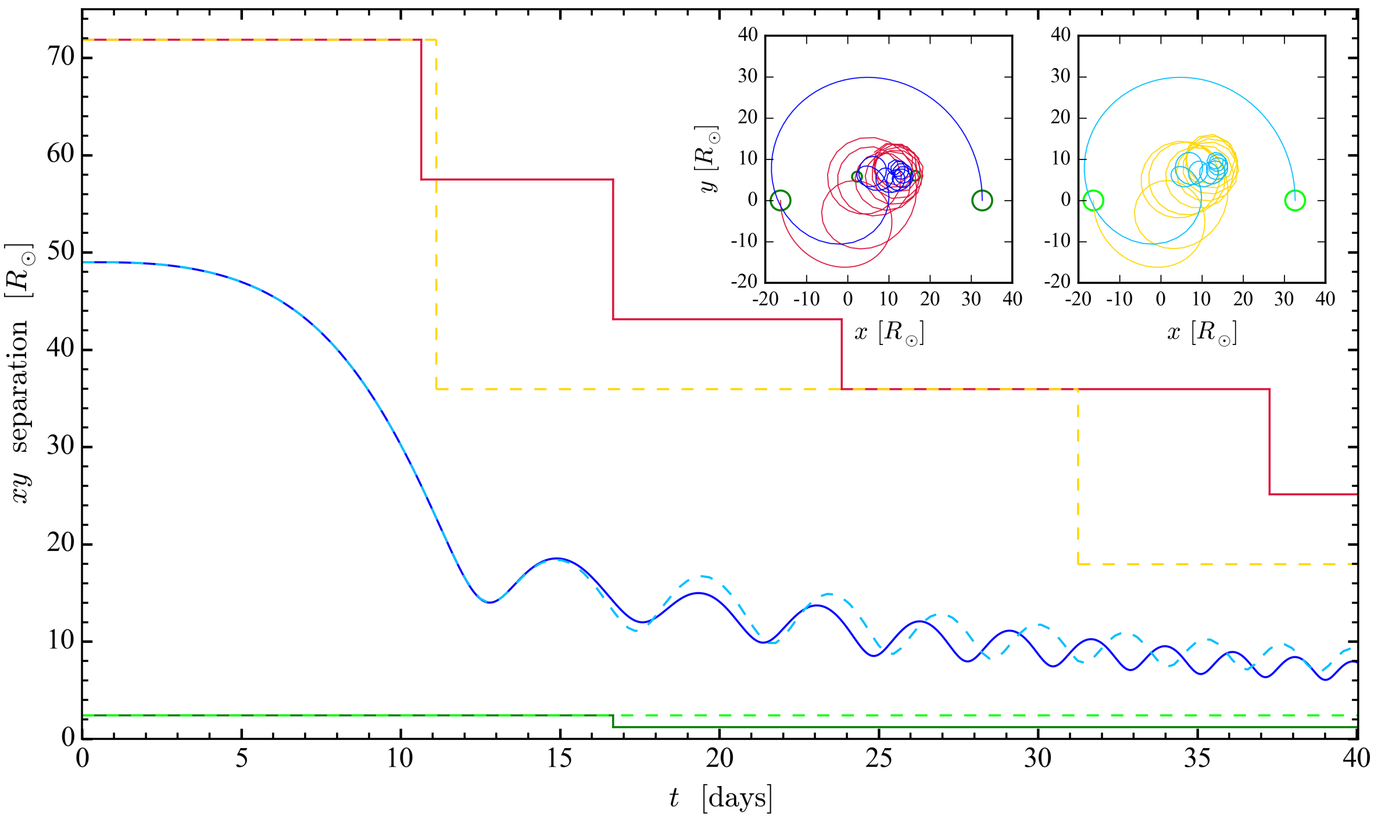

Figure 18: $a(t)$ for Runs 143 and 132.